Trace generation of friction stir welding robot for space weld joint on large thin-walled parts

Ruolong Qi
Shenyang Institute of Automation, Chinese Academy of Sciences, Shenyang, China and
University of Chinese Academy of Sciences, Beijing, China, and
Weijia Zhou, Huijie Zhang, Wei Zhang and Guangxin Yang
Shenyang Institute of Automation, Chinese Academy of Sciences, Shenyang, China

Abstract

Purpose – The weld joint of large thin-wall metal parts which deforms in manufacturing and clamping processes is very difficult to manufacture for its shape is different from the initial model; thus, the space normals of the part surface are uncertain.

Design/methodology/approach – In this paper, an effective method is presented to calculate cutter location points and to estimate the space normals by measuring some sparse discrete points of weld joint. First, a contact-type probe fixed in the end of friction stir welding (FSW) robot is used to measure a series of discrete points on the weld joint. Then, a space curve can be got by fitting the series of points with a quintic spline. Second, a least square plane (LSP) of the measured points is obtained by the least square method. Then, normal vectors of the plane curve, which is the projection of the space curve on the LSP, are used to estimate the space normals of the weld joint curve. After path planning, a post-processing method combing with FSW craft is elaborated.

Findings – Simulation and real experiment demonstrate that the proposed strategy, which obtains cutter locations of welding and normals without measuring the entire surface, is feasible and effective for the FSW of large thin-walled complex surface parts.

Originality/value – This paper presents a novel method which makes it possible to accurately weld the large thin-wall complex surface part by the FSW robot. The proposed method might be applied to any multi-axes FSW robot similar to the robot studied in this paper.

Keywords Path planning, Friction stir welding, Robot welding, Weld joint measurement

Paper type Technical paper

1. Introduction

The large thin-walled complex surface alloy parts are widely used in aeronautics and astronautics, large-scale marines and the other upper manufacturing fields (Shepherd, 2003). But, friction stir welding (FSW) of these large thin-walled parts is challenging for the reasons as follows:

- Most of classic machining cuts off material from work blanks which are larger than the final ideal parts. So, the tool path can be planned based on actual models. No matter which position in the work blank machine cuts from, there is always a high precision part, if only the work blank is large enough (Dai and Serebrennikof, 1996). But, the welding is different, the coordinate relationship between weld joint and machine coordinate have to be confirmed accurately (Crawford *et al.*, 1973).
- The large thin-wall part distorts and deforms in the process of impact extrusion, manufacturing and clamping processes, so the path planned by model is not practical any more (Luan *et al.*, 2006).
- The FSW tools have to be kept at a constant angle to the surface of parts precisely in the process of FSW. Also, it is very difficult to confirm the space normal vector when the ideal part model can not be used for the reason in stated above. (Lv *et al.*, 2013).
- Most of the parts welded by FSW are aluminum or titanium parts with big reflectivity, and they are very difficult to measure by laser or visual sensors.

On the one hand, when measuring with those sensors, the measuring trajectory has to be planned to keep the sensors within effective measurement ranges and in specific postures. For the other hand, the measure precision of laser and visual sensors can be frequently and easily influenced by ambient light and relative location between sensors and parts. The laser or visual sensors also have the defaults of low precision in measure principle, demanding maintenance and hard standardization before use (He *et al.*, 2013).

The current issue and full text archive of this journal is available on Emerald Insight at: **www.emeraldinsight.com/0143-991X.htm**

Industrial Robot: An International Journal
43/6 (2016) 617–627

[DOI 10.1108/IR-04-2015-0075]

The authors are grateful to be supported by the National Science and Technology Major Project of China (2010ZX04007-011) and National Natural Science Foundation of China (Grant No. 51505471).

Received 16 April 2015
Revised 3 December 2015
Accepted 4 December 2015

Industrial Robot: An International Journal
Volume 43 · Number 6 · 2016 · 617–627

Currently, most of the weld joints in plane can be welded by three-axes FSW machine tool. But, large thin-walled complex surface parts are still welded manually, which spend several days to clamp and to weld point by point carefully. Not only the efficiency but also the quality of the artificial weld joint is hard to guarantee. China FSW Center (Beijing FSW Technology Co, Ltd) has developed various of FSW machine tools. Most of them are all special-purpose equipment for a given part. They design high-precision fixtures fixing and amending the distortion of parts to improve the precision of FSW. With the high-precision fixtures, they use the model-based path planning method directly. Most countries including the USA use this method to weld large surface weld joints. Admittedly, it is a high-cost way. Sometimes, the cost of a set of fixtures is nearly equal to the machine tool. NASA is developing a weld joint tracing system; they add a rotation axis and a contacting analog probe to scan the adjacent surface of the weld joint and identify the position of weld joint and fit surface, calculate vectors of surface and interpolate tool positions in real time (Fleming *et al.*, 2010). The weld joint scanning system itself is a complex system which is very hard to design and needs a higher requirement on control system, data communication and computer-aided design (CAD) algorithms.

Even in the process of machining plane weld joint, a tiny distortion of the work piece which is not considered in path planning would cause a serious weld defect. Many researchers spare no efforts on promoting accuracy of FSW. To this end, Okawa *et al.* (2006) used a three-dimensional (3D) coordinate measurement instrument to measure the surface of work piece and weld joint and processed the data in commercial software. This method can be used to machine small parts. When work pieces become larger, a vast number of points on the part surface have to be measured. Soron and Kalaykov (2007) adapted an industry robot to generate 3D welding trajectory of complex parts. They used non-deformable parts and a definitive model. Different from them, many researches focused on the path compensation method (Wang *et al.*, 2004; Longhurst *et al.*, 2010a; Mendes *et al.*, 2014). They fixed a force sensor on the end of the FSW tool and implemented force feedback control as an outer force control loop around the ordinary position control system of a robot manipulator. When the force became larger, the *Z*-axis lifted. But, this method only monitored the position accuracy of the *Z*-axis. The vector direction of FSW tool and the other movement freedoms still relied on the path planning algorithm. Similarly, some other research (Longhurst *et al.*, 2010b,2010c; Davis *et al.*, 2011; Jiang *et al.*, 2011) paid close attention to the force of the feed direction. After many experiments, Longhurst *et al.* (2013) draw a conclusion that using traverse speed instead of plunge depth as the controlling variable provides much greater accuracy in maintaining a desired axial force. Lammlein *et al.* (2012) welded an ideal revolved body without complex trace planning process. Because the action of industry robot has flexible characters, it is more and more used in the FSW. Soron and Kalaykov (2006) describe their approach to modify and provide an industrial robot with FS-welding capacity by modifying a standard industrial robot through replacing its sixth axis with FSW related equipment. The control architecture between force and position sensors and industry robot has been established (Bres *et al.*, 2010). A force and position hybrid control method (Backer *et al.*, 2012) on plane indicates that the force and position hybrid control method could reduce more defections than single force feedback control or single position compensation. Longhurst *et al.* (2011) identifies the key enablers for successful and stable force control of FSW. He put forward that the most important enabler is the maintaining of the position of a portion of the tool's shoulder above the work piece surface. But, when the shoulder is completely submerged below the surface, an unstable system occurs. The other key enablers are a smooth motion profile, an increased lead angle, and positional constraints for the tool. To sum up, there has not been much research on the FSW path planning of large thin-wall parts.

Our approach is measuring a series of discrete points of the weld joint on large thin-walled surface with a contact-type probe fixed in the end of FSW robot. Then, a space curve with a distance of probe radius above real weld joint can be got by fitting the series of points with a quintic spline. The reason why quintic spline is used to describe weld joint is that the quintic spline has higher-order continuity and less curvature than cubic spline. So, with the same number of measure points to fit a curve, a quintic spline is more smooth than a cubic spline. Then, without measuring surface features, an algorithm is proposed to estimate the normal vector of the FSW tool by the measure points. A least square plane (LSP) of the measure points and the projection of the space curve on the LSP are used to estimate the space normal of the weld joint curve. Pseudo-cutter location points dispersed by the chord height error algorithm are moved a distance of a probe radius along the direction of their space normals to get the real cutter locations points. After a post-processing method combing with FSW craft, simulation and real experiment are taken to demonstrate the efficiency of our strategy proposed in this paper.

The rest of this article is structured as follows. Section 2 gives a short elaboration of the FSW robot designed by us. In Section 3, we will develop a measure method, spline fitting formulations and a normal vector estimation algorithm. A post-processing method combing with FSW craft is introduced in Section 4. In Section 5, a simulation is used to certify the precision of the algorithm, and FSW experiment result photos are exhibited. Conclusion and discussion are in Section 6.

2. Friction stir welding robot and thin-walled work piece

What we design is a large dimension robot with seven axes, which also looks like a machine tool. FSW robot designed by us is introduced first. Later, the fixture and work piece are also demonstrated.

2.1 Friction stir welding robot

The FSW robot developed by us (Figure 1) has seven axes. Its general assembly drawing is shown in Figure 2.

The axis definition is according to the tradition of robot, not as same as machine tools. *X*, *Y*, *Z* and *W* are stretch axes, and *A*, *B* and *C* are rotate axes. *X*, *Y*, *Z*, *A* and *B* move together to generate a long definitive trajectory. *C* moves to change the working position to the next one when a weld joint is done. *W*

Figure 1 Photo of FSW robot and thin-walled work piece

Figure 2 General assembly drawing of FSW

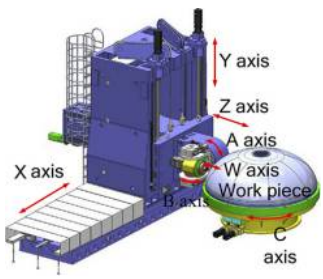

is a high-precision feed axis which is used to insert FSW tool along the direction of normal vector into work pieces at the beginning of welding. The insert movement can be also done by the combined movement of *X*-, *Y*-, *Z*-, *A*- and *B*-axes. But, as the five axes are very large and have geometry error in structure, it is better to do it by *W*-axis, which is a high-precision axis. So, the *W*-axis can be seen as a redundant axis of FSW robot only used in insert feed currently. But, in the future, it will be used to establish a close-loop control with force sensors.

Because the *C*-axis is a single axis now, out of the united feeding of *X*, *Y*, *Z*, *A* and *B*. In the future research, the *C*-axis will be included in the united motion when processing the other weld joints such as horizontal circles. Even though the *W*-axis is a redundant axis, it is only used in insert motion. The motion of *W*-axis will be planned in the process of code generation after path planning.

2.2 Fixture and work pieces

The sketch map of fixture and work pieces is shown in Figure 3. The fixture is low-cost and rough produced by sheet metal parts and weld assembly. The work piece made by 2414-T6 aluminum alloy and is a large distorting sheet of nearly 0.6 cm of thickness. Two pieces of work piece are clamped together by the fixture to form a butt weld which is 1.6 m in length.

3. Trajectory planning

What we desire is an FSW tool path which involves discrete intensive tool location points and corresponding normal vectors of the part surface on these points. So, there are three steps: weld joint measurement, weld joint fitting and normal vector estimation.

Figure 3 Fixture and work pieces

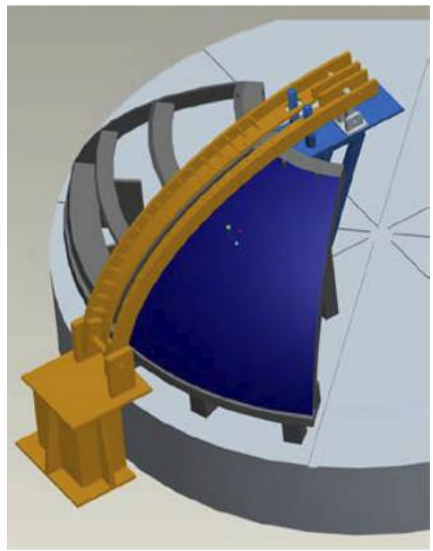

3.1 Weld joint measurement

The low-cost, high-precision trigger type probe (Type id: TP230) produced by Heidenhan Corporation is used in our research. It can be seen as a sensor which outputs a TTL signal immediately when it contacts with something. The principle of the measurement is shown in Figure 4. The robot controller will read grating scale in every interrupt control period and keep the positions of each axis in a buffer. A PC which is used to do path planning offline gets the positions in the buffer of robot controller by OPC protocols (Shi *et al.*, 2011) and calculates the center position of the probe by forward kinematics. Kinematics problem is a basic problem (Qi *et al.*, 2013, 2014a). The sketch map of weld joint measurement is shown in Figure 5. For relationship of the axis positions and the end of robot is a many-to-one mapping, and we can justify different postures to measure the same point and get the same result.

As shown in Figure 5, what we get in the measurement process is not the actual position of the point on the weld joint.

Figure 4 Coordinates of D-H notation for FSW robot

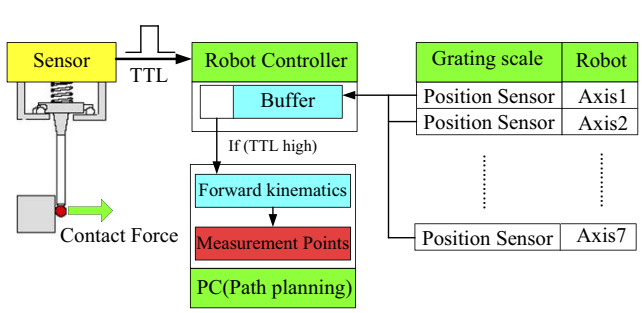

Figure 5 Sketch map of weld joint measurement

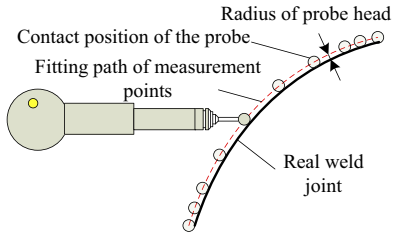

Because the end of the probe is a small ball, the measurement value calculated by forward kinematics is the position above the point on the weld joint with a radius distance in the normal direction of the surface.

Then, with the proposed method, the points on the weld joint can be measured one by one. With the algorithms elaborated in the next two Sections 3.2 and 3.3, even though not too many points are measured, a long path can be still planned well.

3.2 Friction stir welding tool location calculation

3.2.1 Measure points fitting

In principle, the more points measured, the more accurate the fitting curve is. But, under real circumstance, more measures mean that more measurement errors are added into the measurement coordinates. Also, because the work piece is very large and the desire is to save measure time, it is better to measure a set of sparse points. To this end, a space quintic spline algorithm that is based on the tangent vector of the cubic spline is proposed. So, a cubic spline is fitted by the points first and a quintic spline is calculated based on it.

It is assumed that the coordinates got by the method proposed in Section 3.1 are $[P_1, P_2, P_3, [\ldots] [\ldots], P_n]$. The spline that connected point $P_{i-1}(x_{i-1}, y_{i-1}, z_{i-1})$ and $P_i(x_i, y_i, z_i)$ can be fitted by the four points: P_{i-1}, P_i, P_{i+1} and P_{i+2} with equation (1).

$$P_i(u) = a_i u^3 + b_i u^2 + c_i u + d_i, \tag{1}$$

where parameter u is a variable from zero to the length of chord l_{i-1} that connected points P_{i-1} and P_i. Define two new symbol $l_{i-1,\,i} \triangleq$ and $l_{i-1,\,i+1} \triangleq$ to express the cumulative sum of several sequential chord lengths. $l_{i-1,\,i} \triangleq l_{i-1} + l_i$ and $l_{i-1,\,i+1} \triangleq l_{i-1} + l_i + l_{i+1}$:

$$l_{i-1} = \sqrt{(x_i - x_{i-1})^2 + (y_i - y_{i-1})^2 + (z_i - z_{i-1})^2} \tag{2}$$

The parameters a_i, b_i, c_i and d_i in equation (1) can be calculated as:

$$a_i = \frac{1}{\boldsymbol{\Delta}}\begin{bmatrix}\boldsymbol{\Delta}_{ax}\\ \boldsymbol{\Delta}_{ay}\\ \boldsymbol{\Delta}_{az}\end{bmatrix}, b_i = \frac{1}{\boldsymbol{\Delta}}\begin{bmatrix}\boldsymbol{\Delta}_{bx}\\ \boldsymbol{\Delta}_{by}\\ \boldsymbol{\Delta}_{bz}\end{bmatrix}, c_i = \frac{1}{\boldsymbol{\Delta}}\begin{bmatrix}\boldsymbol{\Delta}_{cx}\\ \boldsymbol{\Delta}_{cy}\\ \boldsymbol{\Delta}_{cz}\end{bmatrix}, d_i = \frac{1}{\boldsymbol{\Delta}}\begin{bmatrix}\boldsymbol{\Delta}_{dx}\\ \boldsymbol{\Delta}_{dy}\\ \boldsymbol{\Delta}_{dz}\end{bmatrix} \tag{3}$$

$$\begin{aligned}
\boldsymbol{\Delta} &= \begin{vmatrix} l^3_{i-1} & l^2_{i-1} & l_{i-1} \\ l^3_{i-1,i} & l^2_{i-1,i} & l_{i-1,i} \\ l^3_{i-1,i+1} & l^2_{i-1,i+1} & l_{i-1,i+1} \end{vmatrix} \\
\boldsymbol{\Delta}_{ax} &= \begin{vmatrix} x_i - x_{i-1} & l^2_{i-1} & l_{i-1} \\ x_{i+1} - x_{i-1} & l^2_{i-1,t} & l_{i-1,i} \\ x_{i+2} - x_{i-1} & l^2_{i-1,i+1} & l_{i-1,i+1} \end{vmatrix} \\
\boldsymbol{\Delta}_{bx} &= \begin{vmatrix} l^3_{i-1} & x_i - x_{i-1} & l_{i-1} \\ l^3_{i-1,i} & x_{i+1} - x_{i-1} & l_{i-1,i} \\ l^3_{i-1,i+1} & x_{i+2} - x_{i-1} & l_{i-1,i+1} \end{vmatrix} \\
\boldsymbol{\Delta}_{cx} &= \begin{vmatrix} l^3_{i-1} & l^2_{i-1} & x_i - x_{i-1} \\ l^3_{i-1,i} & l^2_{i-1,i} & x_{i+1} - x_{i-1} \\ l^3_{i-1,i+1} & l^2_{i-1,i+1} & x_{i+2} - x_{i-1} \end{vmatrix}
\end{aligned} \tag{4}$$

In a similar way, the parameters $\boldsymbol{\Delta}_{ay}\boldsymbol{\Delta}_{by}\boldsymbol{\Delta}_{cy}$ and $\boldsymbol{\Delta}_{az}\boldsymbol{\Delta}_{bz}\boldsymbol{\Delta}_{cz}$ in equation (3) could be got by replacing $(x_i - x_{i-1})$ with $(y_i - y_{i-1})$ and $(z_i - z_{i-1})$.

The first- and second-order derivatives at P_i are calculated as:

$$\left\{\begin{aligned} t_i &\triangleq \begin{bmatrix} t_{xi} \\ t_{yi} \\ t_{zi} \end{bmatrix} = \frac{dP_i}{du}\Big|_{u=l_{i-1}} = (3a_i u^2 + 2b_i u + c_i)\Big|_{u=l_{i-1}} \\ n_i &\triangleq \begin{bmatrix} n_{xi} \\ n_{yi} \\ n_{zi} \end{bmatrix} = \frac{d^2P_i}{du^2}\Big|_{u=l_{i-1}} = (6a_i u + 2b_i)\Big|_{u=l_{i-1}} \end{aligned}\right\} \tag{5}$$

Because of the lack of extra neighboring points, the first- and second-order derivatives at P_1, P_{n-1} and P_n are estimated using the cubic polynomials [equations (6)-(8)].

$$t_1 = 3a_2u^2 + 2b_2u + c_2, n_1 = 6a_2u + 2b_2 \quad u = 0 \tag{6}$$

$$\begin{aligned} t_{N-1} &= 3a_{N-2}u^2 + 2b_{N-2}u + c_{N-2}, \\ n_{N-1} &= 6a_{N-2}u + 2b_{N-2} \quad u = l_{N-3} + l_{N-2} \end{aligned} \tag{7}$$

$$\begin{aligned} t_N &= 3a_{N-2}u^2 + 2b_{N-2}u + c_{N-2}, \\ n_N &= 6a_{N-2}u + 2b_{N-2} \quad u = l_{N-3} + l_{N-2} + l_{N-1} \end{aligned} \tag{8}$$

Once the first and second derivatives at the measurement points are determined, a quintic spline in the same form with equation (1) is written as:

$$S_i(u) = A_i u^5 + B_i u^4 + C_i u^3 + D_i u^2 + E_i u + F_i \tag{9}$$

$$S_i = \begin{bmatrix} S_{xi} \\ S_{yi} \\ S_{zi} \end{bmatrix}, A_i = \begin{bmatrix} A_{xi} \\ A_{yi} \\ A_{zi} \end{bmatrix}, B_i = \begin{bmatrix} B_{xi} \\ B_{yi} \\ A_{zi} \end{bmatrix}, \cdots, F_i = \begin{bmatrix} F_{xi} \\ F_{yi} \\ A_{zi} \end{bmatrix} \tag{10}$$

With the boundary equations (6)-(8), A_i, B_i, C_i, D_i, E_i and F_i are obtained:

$$
\begin{aligned}
A_{xi} &= \frac{1}{l_i^5}[6(x_{i+1} - x_i) - 3(t_{x,i+1} + t_{xi}) + 0.5(n_{x,i+1} - n_{xi})l_i^2] \\
B_{xi} &= \frac{1}{l_i^4}[15(x_i - x_{i+1}) + (7t_{x,i+1} + 8t_{xi})l_i + (1.5n_{x,i+1} - n_{xi})l_i^2] \\
C_{xi} &= \frac{1}{l_i^3}[10(x_{i+1} - x_i) - (4t_{x,i+1} + 6t_{xi}) - (1.5n_{xi} - 0.5n_{x,i+1})l_i^2] \\
D_{xi} &= 0.5n_{xi} \\
E_{xi} &= t_{xi} \\
F_{xi} &= x_i
\end{aligned} \tag{11}
$$

A_{yi}, B_{yi}, C_{yi}, D_{yi}, E_{yi}, F_{yi}, A_{zi}, B_{zi}, C_{zi}, D_{zi}, E_{zi} and F_{zi} could be got similarly with equation (11) by replacing x_i, t_{xi} and n_{xi} with y_i, t_{yi} and n_{yi} and z_i, t_{zi} and n_{zi}.

So far, we can generate a quintic spline of measurement points by the above algorithm. However, the spline is not the weld joint but a curve with a radius distance above the weld joint in the normal direction of the part surface. For the convenience of expression, the quintic spline is named as pseudo-path. With the "chord height error" algorithm (Qi *et al.*, 2014b), pseudo-path can be dispersed into a series of points, which are called "pseudo FSW location points". That is because no matter how smoothly the robot or CNC system moves, in the inner control systems, they all move a tiny straight line in every interrupt period to approximate the path curve pre-defined. So, the path planning process based on measurement is also the process of fitting points (measure points) to a curve, and dispersing the curve into points (FSW tool location points).

3.2.2 Normal vector estimation

It is well known that FSW claims rigorous requirements on the accuracy of the normal direction and position vertical to the surface. The FSW tool has to be kept at a constant angle with the normal vector, or the metal material could be squeezed out of the part forming serious flaw during weld producing. So, when the measurement of the weld joint cannot provide the surface information, it is important to estimate the normal vector accurately.

The large thin-walled parts distort in all the process of its stamping forging, transportation and clamping on the fixture. The error between real and ideal weld joint is very large. An exaggerated sketch map of distorted weld joint with the two work pieces (red and green) is shown in Figure 6.

First, an LSP is calculated by the pseudo-FSW location points (PSLP) got in Section 3.2.1 to estimate the ideal weld joint location. It is wise to use the PSLP but not the measurement point to fit the LSP. That is because the more points involved in the least square calculation, the more reliable the result is. The parameters A, B and C of LSP ($Ax + By + Cz + 1 = 0$) can be expressed by equation (12) with the coordinate of PSLP [Q_1, Q_2, Q_3 [. . .] Q_i (x_i, y_i, z_i) [. . .], Q_n]:

$$
\begin{bmatrix} A \\ B \\ C \end{bmatrix} = \begin{bmatrix} \Sigma x_i^2 & \Sigma x_i y_i & \Sigma x_i z_i \\ \Sigma x_i y_i & \Sigma y_i^2 & \Sigma y_i z_i \\ \Sigma x_i z_i & \Sigma y_i z_i & \Sigma z_i^2 \end{bmatrix}^{-1} \begin{bmatrix} -\sum_0^n x \\ -\sum_0^n y \\ -\sum_0^n z \end{bmatrix} \tag{12}
$$

Second, project all the PSLP into the LSP, getting the sub-points of PLSP (SPLSP) with equation(13). Getting three points [x_1, y_1, z_1], [x_2, y_2, z_2], [x_3, y_3, z_3] in the LSP randomly, the sub-point coordinate [x_q, y_q, z_q] of a PLSP [x_p, y_p, z_p] can be calculated by equation (13). There is a principle axis of the work piece which is nearly the same with the center line of the C-axis of the robot when fixed in the fixture (Figure 6).

The projective angle α is the angle of PSLP and SPLSP about the principle axis. The angle α can be calculated by geometry easily. Then, all the SPLSP in the LSP are fit with the quintic spline algorithm proposed in Section 3.2.1:

$$
\begin{bmatrix} x_q \\ y_q \\ z_q \end{bmatrix} = \begin{bmatrix} x_2 - x_1 & y_2 - y_1 & z_2 - z_1 \\ x_3 - x_1 & y_3 - y_1 & z_3 - z_1 \\ A & B & C \end{bmatrix}^{-1} \cdot \begin{bmatrix} x_p(x_2 - x_1) + y_p(y_2 - y_1) + z_p(z_2 - z_1) \\ x_p(x_3 - x_1) + y_p(y_3 - y_1) + z_p(z_3 - z_1) \\ -1 \end{bmatrix} \tag{13}
$$

Third, what we want now is the normal vector of pseudo FSW tool location point in plane (Figure 6). The normal vector of the plane (Figure 7) is known as $\vec{v}_n$ = [A, B, C], and the tangent of SPLSP can be calculated when the spline in plane is known to us (done in the above section); $\vec{v}_t$ is just the vector of the point P_1 ($u = u_1$) and P_2 ($u = u_1$ + small) in which "small" is a rational number such as 0.0001. Then, the normal vector of pseudo FSW tool location point in plane $\vec{v}_\tau$ is:

$$
\vec{v}_\tau = \vec{v}_n \times \vec{v}_t \tag{14}
$$

Fourth, the space normal vector $\vec{v}_s$ of the PSLP is easy to be calculated by equation (15) when $\vec{v}_\tau$ and α are known to us:

$$
\vec{\mathbf{v}}_S = \vec{\mathbf{v}}_\tau \cdot \begin{bmatrix} \cos\alpha & -\sin\alpha & 0 \\ \sin\alpha & \cos\alpha & 0 \\ 0 & 0 & 1 \end{bmatrix} \tag{15}
$$

Figure 6 Sketch map of space normal vector evaluation

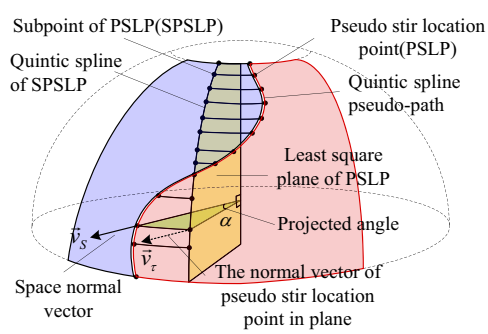

Figure 7 Sketch map of plane normal vector calculation

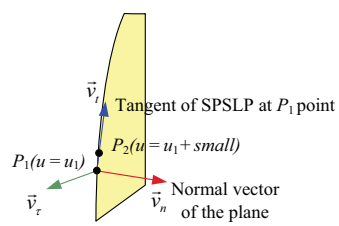

By now, the pseudo FSW tool location points and corresponding normal vectors are calculated. For the pseudo FSW tool location points, [Q_1, Q_2, Q_3 [. . .] [. . .], Q_n] are a radius distance above the real FSW tool location points, it is easy to understand, and the real FSW tool location points [P_1, P_2, P_3 [. . .] [. . .], P_n] can be obtained by equation (16):

$$[P_1, P_2, P_3, ..., P_n] = [Q_1, Q_2, Q_3, ...Q_n] - (\text{radius of probe}) \times \vec{v}_\tau \quad (16)$$

4. Code generation

In this section, a method of translating a planned path in Section 3 with craft requirements into a code file that robot can understand is introduced.

The technological requirement is saved in a database that is connected with path planning and simulation platform (Section 5). When the path planning process is done, the data in the RAM memory are just a queue that save a set of point coordinates with their normal vectors. What we want is to translate these data into a file with crafts that a robot can understand. Even though different control systems have different file input and output systems, only the defined format is what they can read. But what we focus on is the method to translate but not the specific format. The control system used in our research is CNC system, not the professional robot controller. That is because the robot controllers such as KUKA and STAUBLI cannot connect with line grating sensors, which are indispensable for the highly accurate control, especially for our huge FSW robot which has three linear motion axes. So, the file standard in our research is G code, which is well known and easily understood.

The craft used in FSW is summed up in Table I. The FSW tool is fixed on the end of the robot. When the welding begins, the spindle starts running and the end of the robot moves to the position above the first point of the path planned with an approaching distance in the direction of normal vector. Then, it moves to the insert point, which is at an insert distance above the first path point with the approaching speed. After that, the FSW tool will insert into the work piece with the insert speed from the insert point. If the pin or the shoulder of tool need preheat, the FSW tool should stay for the preheat time when the spindle is rotating. Sometimes, in FSW, the FSW tool needs to move at different speeds (the *n*th section feed speed) in different sections (the *n*th section feed distance) according to the arc length of planned path. Generally, the extracting distance and extracting speed are equal to the insert distance and insert speed, respectively, and approaching and leaving distance and speed are also usually the same.

Table I General crafts

No.	Abbreviation	Remarks
1	AD	Approach distance to the work piece
2	AS	Approach speed to the work piece
3	ID	Insert distance to the work piece
4	IS	Insert speed to the work piece
5	SS	Spindle speed
6	NPT	Needle preheat time
7	SPT	Shoulder preheat time
8	SPP	Shoulder press depth
9	FDn	The *n*th section feed distance
10	FSn	The *n*th section feed speed
11	ED	Extracting distance from the work piece
12	ES	Extracting speed from the work piece
13	LD	Leaving distance from the work piece
14	LS	Leaving speed from the work piece

According to the craft, we establish a structure for every point of the path planned and save the structure in a queue which is used to generate the code file. The details of the new structure are shown in Table II.

Then, we change every point planned before into the structure type in Table II and save them into a queue. The process is shown in Table III.

After the post-position process shown in Table III, a queue of path structure integrated with craft is generated. Then, a code file can be generated line by line according to the structure in the queue one by one.

5. Simulation and experiments

The correction and precision of the algorithm proposed in this paper is identified in Section 5.1. The real FSW process and result according to this paper are shown by spot photos.

5.1 Algorithm simulation in VC platform

A path planning and simulation system shown in Figure 8 is developed in VC platform with C++ language.

To identify the accuracy of the algorithm proposed in this paper, the simulation system with no error should measure a foregone shape such as ball, cylinder, etc. After fitting the measured points and planning a path with algorithm introduced in Section 3.2 and comparing the result with the foregone shape, we can identify whether the algorithm is useful.

Because the *A*- and *B*-axes of the robot intersect at one point, when keeping the *X*-, *Y*-, *Z*- and *W*-axes state and moving *A*- and *B*-axes, the end point of the robot should be in a spherical surface. Figure 9 shows the process of getting the end point of the robot by this method. To test how robust the algorithm is, we get only a few points. The length of *A*- and *B*-axes is 700 mm. Figure 10 shows the path planning result and the output data of the simulation system. The same seven measurement points are used to do path planning with cubic spline and quintic spline that are mentioned in Section 3.2, respectively. The comparison of the results is shown in Figures 11 and 12.

The position error of the FSW tool location is shown in Figure 11. The error of the quintic spline is controlled

Table II New structure of the path point

No.	Variable	Type	Remarks
1	m_pos	double*3	Save the position coordinates
2	m_vec	double*3	Save the normal vector
3	m_ifDwell	bool	If the FSW tool dwells awhile
4	m_dwellT	int	Dwell time (unit: s)
5	m_ifFeedC	bool	If the feed speed changes
6	m_feedS	int	Feed speed of FSW tool (unit: mm/s)

Table III Postposition process

No.	Method
0	*Input:* Path points; Craft; New structure; A null queue;
1	Transform all path points into the structure type and add the structures to the queue one by one. So all the variables expect m_pos and m_vec are zeroes
2	Judge if feed speed changes in craft: Do: if $\sum dis(p_i, p_{i+1}) \geq$ the n-th section feed distance m_ifFeedC=1; m_feedS = feed speed; end Not: do nothing end
3	Judge if shaft shoulder press depth of the craft is zero: Do: do nothing Not: a)cope the first structure (m_posfirst and m_vecfirst)and add to the beginning of the queue b)m_pos = m_posfirst- (press depth) * m_vecfirst for every structure from the second structure in the queue end
4	Judge if needs preheating FSW needle by the craft: Do: Add a structure to the beginning of the queue whose m_pos = m_posfirst + 0.5 * (FSW tool length) * m_vecfirst Not: do nothing end
5	Judge if needs preheating shaft shoulder by the craft: Do: Add a structure to the beginning of the queue whose m_pos = m_posfirst + (FSW tool length) * m_vecfirst Not: do nothing end
6	Add a cope structure to the beginning of the queue whose m_pos = m_posfirst + (Insert distance) * m_vecfirst m_ifFeedC = 1; m_feedS = Insert speed;
7	Add a structure to the beginning of the queue whose m_pos = m_posfirst + (Approach distance) * m_vecfirst m_ifFeedC = 1; m_feedS = Approach speed;
8	Add a cope structure to the end of the queue whose m_pos = m_posfirst- (Insert distance) * m_vecfirst m_ifFeedC = 1; m_feedS = Insert speed;
9	Add a cope structure to the end of the queue whose m_pos = m_posfirst- (extracting distance) * m_vecfirst m_ifFeedC = 1; m_feedS= Insert speed;
10	Add a cope structure to the end of the queue whose m_pos = m_posfirst- (leaving distance) * m_vecfirst m_ifFeedC = 1; m_feedS = Insert speed;

Figure 8 Interface of FSW

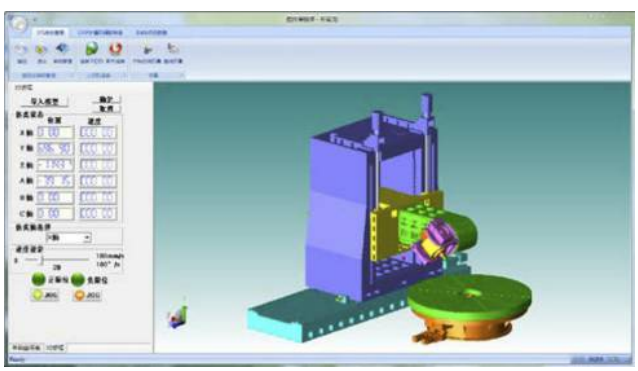

Figure 9 Measurement in simulation system

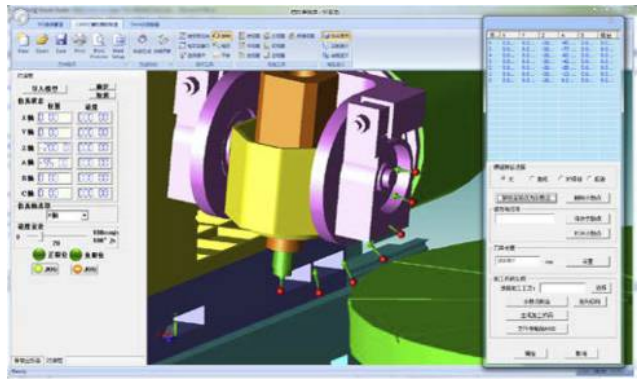

Figure 10 Data output of simulation system

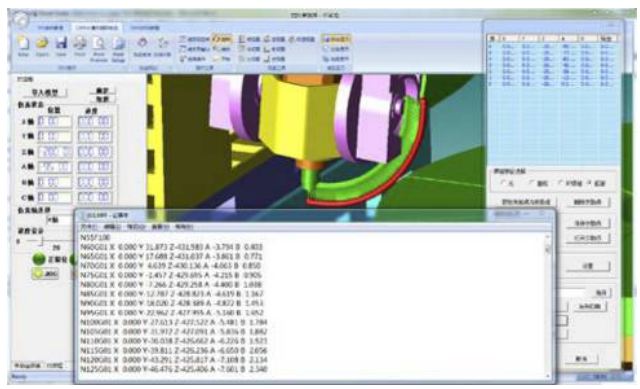

Figure 11 Path planning position error (unit: mm)

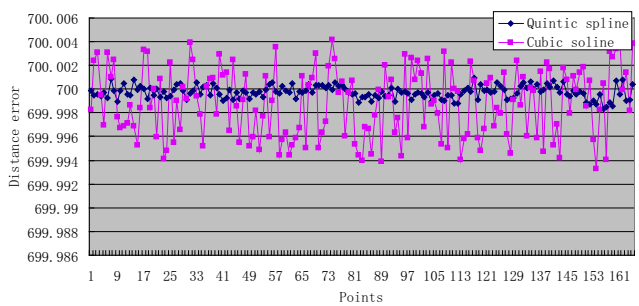

Figure 12 Path planning angle error (unit: degree)

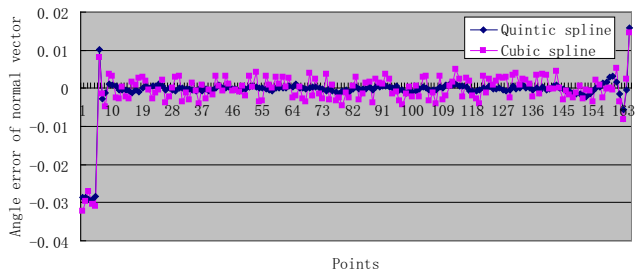

between ±15 μm when the error of the cubic spline is ±60 μm. Most of the angle error of the normal vector direction is controlled at ±0.003°. But, the angle error of cubic spline is larger and is mostly about ±0.005°.

The precision index of the end of FSW robot includes two parts: position precision and angle precision, which are the design targets to satisfy the FSW craft. The position precision index is ±0.05 mm, and the angle precision is ±0.5°. The motion error of the end point of the FSW robot includes two main factors. One is the error of the mechanical structure, which includes many factors such as manufacturing error, assembling error, distortion error of large structural component, etc. The other one is the path planning error. According to the engineering experience, path planning error should less than one-tenth of mechanical structure error. So, the path planning error of position should less than ±0.005 mm, and the angle error should less than ±0.05°. So, according to the simulation result, both the quintic spline and the cubic spline satisfy the precision index of the path planning error. But, the quintic spline is better for its smaller error.

At the beginning and the end of the path, the errors of both methods are similar and a little larger (about ± 0.03°), because the first- and second-order derivatives of quintic spline are estimated by the cubic spline. At the beginning and the end of the spline curve, the derivatives are not that accurate because of the lack of mathematic constraint. This phenomenon will also be discussed in conclusion.

5.2 Real friction stir welding machining experiment

The work pieces used in the FSW machining experiment are two pieces of large sheets made by 2A14-T6 AL which are 0.6 cm in thickness. The two pieces of sheets are clamped together to form a 1.6-m-long butt weld, as shown in Figure 13. We get the measurement points nearly every 10 cm distance on the work piece. To measure points on the weld joint evenly, marking pen can be used to draw some marks on the work pieces to indicate that the positions are to be measured. When measuring every point, we hold the control panel in hand to control the robot moves to be close to the weld joint. The process is controlled manually and animated by the eyes of the controller. When the probe is fixed in the end of the robot contacted with the weld joint, the robot will record the axis positions with the method proposed in Section 3.1.

Under ideal conditions, when measuring one point, the probe should be exactly on the weld joint, as shown in Case 1

Figure 13 The butt weld to measure

Figure 14 The weld joint measurement process

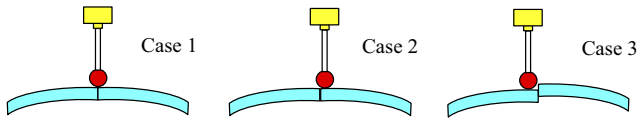

Figure 15 Sketch map of FSW process with measurement deviation from weld joint

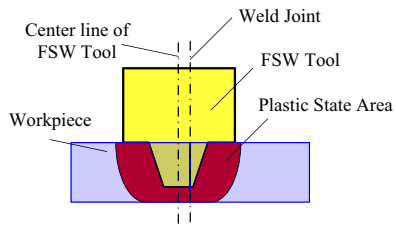

Figure 16 The weld joint measurement process

(a)

(b)

of Figure 14. But, under real conditions, the probe could not contact the weld joint exactly because of two main reasons. One reason is the visual error of controller who measures the weld joint, as shown in Case 2 of Figure 14. The other reason is the less-than-ideal clamping of work pieces, as shown in Case 3 of Figure 14. For the distort of work pieces, some place of the weld joint is uneven. At this place, the point near the weld joint on the lower part should be chosen as the measurement point.

Even though the measurement points are measured manually and inevitably have some errors in the direction perpendicular to that of the weld joint on the surface of work pieces, the impact on the quality of FSW is limited if only the measurement precision in the normal direction of the work piece surface is guaranteed by the method proposed in Section 3.1. That is because the FSW craft has high position precision requirement in the normal direction of work piece, but the precision requirement of the other direction is not that high if only the width of plastic state area generated in the machining process of FSW is larger than the error of measurement (Figure 15).

The measurement process is shown in Figure 16. All the measurement points are fitted by quintic spline (Figure 17). The work piece is machined with a zero tool tilt angle. That is to say, the FSW needle is perpendicular to the surface of the work piece in the process of FSW machining. The real FSW machining process is shown in Figure 18, and the result of FSW machining is shown in Figure 19. Figure 19 indicates that the large thin-walled aluminum component has been successfully friction stir welded by the approach

Figure 17 The points fitting by path planning system

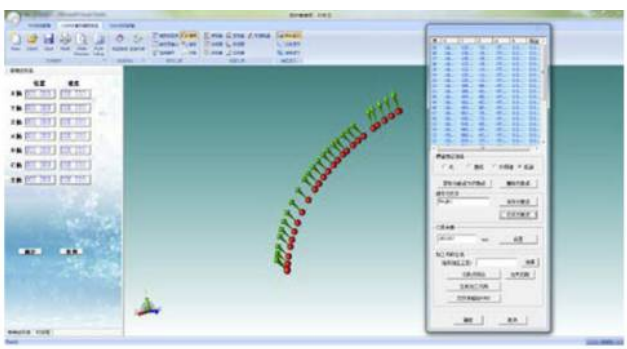

(a)

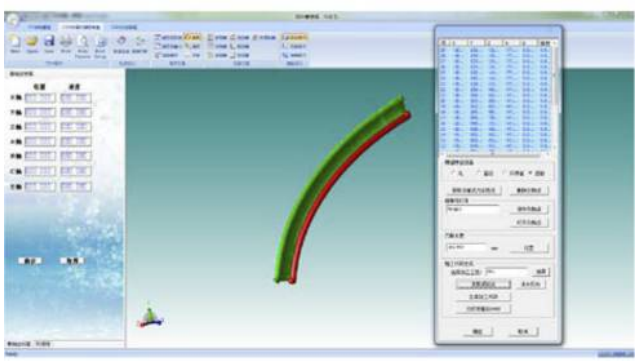

(b)

Figure 18 The FSW machining process

(a)

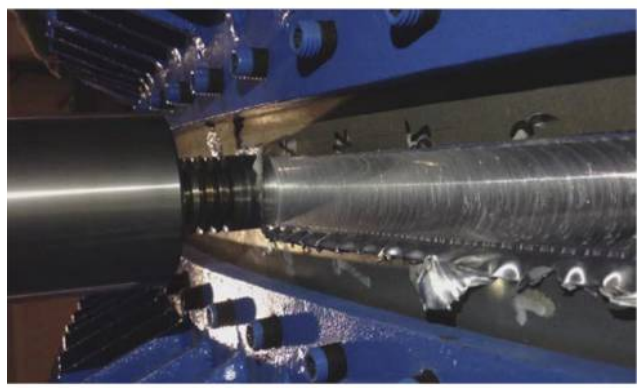

(b)

presented in this paper. The smooth weld track characterized by homogenous onion rings suggests a high formation quality on weld top surface. The FSW joint was also cross-sectioned to evaluate the inner quality of the weld formation, as shown in Figure 20. Apparently, a dense and integrated nugget zone is formed in the weld, and no welding defects are observed in the inner part of weld, this further confirms the feasibility of the measuring approach of weld track proposed in this paper.

6. Conclusions

The conclusions are as follows:

- To solve the distortion and deform problem of the large thin-walled part, an effective method is presented to calculate cutter location points and estimate the space normals by measuring the sparse discrete points on weld joint. Simulation and experiment prove that the algorithm proposed in this paper is useful and effective.
- At the beginning and the end of the path, the error of normal vectors estimated by our algorithm is larger than the other path points. That is because the first- and second-order derivative of the first and the last two measure points are estimated by the nearest spline curve because of the lack of adjacent points. Measuring high-density points at the beginning and the end of the weld joint is useful to improve the error of normal vectors.

Figure 19 The FSW result

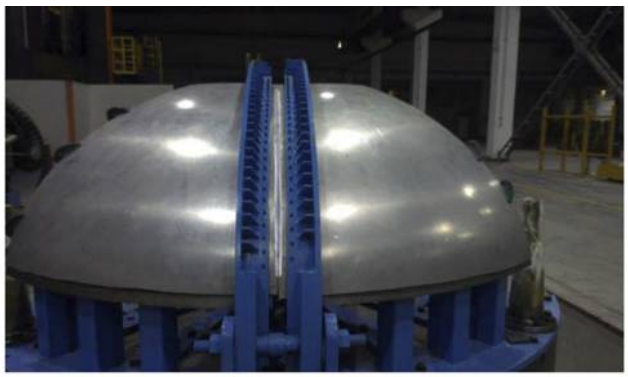

(a)

(b)

Figure 20 Cross-section of the weld

- If not considering the error of measurement, in principle, more measure points on the weld joint would increase the accuracy of fitting curve.
- The method proposed in this paper could be used at the other machining fields or with different tools such as loxodrome coolant channel machining on liquid rocket engine with a flack cutter, missile radome grinding or other machining on complex surface. The advantage of the method proposed in this paper is improving path planning for complex geometries based on simple measurement of a real part rather than idealized CAD geometries.
- In the future, there are three critical technologies yet to be solved. The first one is to measure and analyze how much distortion and deformation occurs before machining and during machining. The second one is to realize the automatic measurement. The third one is to use the method proposed in this paper to the other components and even the other field.

References

Backer, J.D., Christiansson, A.K., Oqueka, J. and Bolmsjö, G. (2012), "Investigation of path compensation methods for robotic friction stir welding", *Industrial Robot: An International Journal*, Vol. 39 No. 6, pp. 601-608.

Bres, A., Monsarrat, B., Dubourg, L., Birglen, L., Perron, C. and Jahazi, M. and Baron, L. (2010), "Simulation of friction stir welding using industrial robots", *Industrial Robot: An International Journal*, Vol. 37 No. 15, pp. 36-50.

Crawford, R., Strauss, A.M., Cook, G.E. and Clark, D.E. (1973), "Robotic friction stir welding", *Industrial Robot: An International Journal*, Vol. 31 No. 1, pp. 55-63.

Dai, Y. and Serebrennikof, G.Z. (1996), "The synthetical quality control for complicated shape parts processing under high-load in aircraft engine", *Journal of National University of Defense Technology*, Vol. 18 No. 3, pp. 59-62.

Davis, T.A., Ngo, P.D. and Shin, Y.C. (2011), "Multi-level fuzzy control of friction stir welding power", *International Journal of Advanced Manufacturing Technology*, Vol. 59 Nos 5/8, pp. 559-567.

Fleming, P.A., Hendricks, C.E., Cook, G.E., Wilkes, D.M., Strauss, A.M. and Lammlein, D.H. (2010), "Seam-tracking for friction stir welded lap joints", *Journal of Materials Engineering and Performance*, Vol. 19 No. 8, pp. 1128-1132.

He, H.L., Lei, X.C., Gong, Y.F. and Zhao, C. (2013), "Research on a seam tracking system based on laser vision sensor measuring", *Control Engineering of China*, Vol. 20 No. 5, pp. 869-872.

Jiang, M.L., Wang, M. and Tian, F.J. (2011), "Monitoring system design of FSW", *Welding Technology*, Vol. 40 No. 12, pp. 35-39.

Lammlein, D.H., Gibson, B.T., Delapp, D.R., Cox, C., Strauss, A.M. and Cook, G.E. (2012), "The friction stir welding of small-diameter pipe: an experimental and numerical proof of concept for automation and manufacturing", *Proceedings of the Institution of Mechanical Engineers, Part B: Journal of Engineering Manufacture*, Vol. 226 No. B3, pp. 383-398.

Longhurst, W.R., Strauss, A.M. and Cook, G.E. (2010a), "Enabling automation of friction stir welding: the modulation of weld seam input energy by traverse speed force control", *Journal of Dynamic Systems Measurement & Control*, Vol. 132 No. 4, pp. 041002.1-041002.11.

Longhurst, W.R., Strauss, A.M. and Cook, G.E. (2011), "The identification of the key enablers for force control of robotic friction stir welding", *Journal of Manufacturing Science & Engineering*, Vol. 133 No. 3, pp. 255-267.

Longhurst, W.R., Strauss, A.M. and Cook, G.E. (2013), "Enabling automation of friction stir welding: the modulation of weld seam input energy by traverse speed force control", *Journal of Dynamic Systems Measurement & Control*, Vol. 132 No. 4, pp. 1-11.

Longhurst, W.R., Strauss, A.M., Cook, G.E., Cox, C.D., Hendricks, C.E. and Gibson, B.T. (2010b), "Investigation of force-controlled friction stir welding for manufacturing and automation", *Proceedings of the Institution of Mechanical Engineers, Part B: Journal of Engineering Manufacture*, Vol. 224 No. 6, pp. 937-949.

Longhurst, W.R., Strauss, A.M., Cook, G.E. and Fleming, P.A. (2010c), "Torque control of friction stir welding for manufacturing and automation", *International Journal of Advanced Manufacturing Technology*, Vol. 51 Nos 9/12, pp. 905-914.

Luan, G.H., Hu, H.H. and Chai, P. (2006), "Friction stir welding-innovative vehicle manufacturing process", *Electric Locomotives & Mass Transit Vehicles*, Vol. 29 No. 4, pp. 40-44.

Lv, X.Q., Zhang, K. and Wu, Y.X. (2013), "Seam tracking control for mobile welding robots based on dynamic model", *Transactions of the China Welding Institution*, Vol. 34 No. 10, pp. 13-16.

Mendes, N., Neto, P., Simão, M.A., Loureiro, A. and Pires, J.N. (2014), "A novel friction stir welding robotic platform: welding polymeric materials", *International Journal of Advanced Manufacturing Technology*, Vol. 85 No. 1, doi: 10.1007/s00170-014-6024-z.

Okawa, Y., Taniguchi, M., Sugii, H. and Marutani, Y. (2006), "Development of 5-axis friction stir welding system", *SICE-ICASE International Joint Conference*, *Bexco*, pp. 1266-1269.

Qi, R.L., Zhou, W.J., Liu, J.G. and Xiao, L. (2013), "An effective method for implementing virtual control and 3D simulation of robot motion in VC platform", *Robot*, Vol. 35 No. 5, pp. 594-599.

Qi, R.L., Zhou, W.J. and Wang, T.J. (2014a), "An obstacle avoidance trajectory planning scheme for space manipulators based on genetic algorithm", *Robot*, Vol. 36 No. 3, pp. 263-270.

Qi, R.L., Zhou, W.J., Zhang, W. and Zhang, X. (2014b), "Measurement and trace generation of a friction stir welding robot for space weld joint on large thin-walled parts", *Robot*, Vol. 36 No. 6, pp. 744-750.

Shepherd, G. (2003), "The evaluation of friction stir welded joints on airbus aircraft wing structure", *4th International Friction Stir Welding Symposium*, Park City, UT, pp. 1-5.

Shi, L., Hua, B., Zhu, X. and Wu, M. (2011), "Real-time communication between PC and Siemens PLC based on OPC", *Marine Electric & Electronic Technology*, Vol. 31 No. 1, pp. 9-12.

Soron, M. and Kalaykov, I. (2006), "A robot prototype for friction stir welding", *IEEE Conference on Robotics, Automation and Mechatronics*, Bangkok, pp. 1-5.

Soron, M. and Kalaykov, I. (2007), "Generation of continuous tool paths based on CAD models for friction stir welding in 3D", *Material Conference on Control and Automation*, *Athens*, pp. 1-5.

Wang, X.J., Zhang, Z.K., Guo, R.J., Han, X.H. and Rong, A. (2004), "Application of MCGS for process control and realtime detection in the process of friction stir welding", *8th International Conference on Control, Automation, Robotics and Vision*, Kunming, Yunnan, pp. 499-503.

About the authors

Ruolong Qi (born in 1983) is currently a PhD Candidate at University of Chinese Academy of Sciences and an Associate Professor at State Key Laboratory of Robotics, Shenyang Institute of Automation, Chinese Academy of Sciences, China. He received his bachelor's and master's degree from Dalian University of Technology, China, in 2005 and 2008, respectively. His research interests include robot system and intelligent robotics.

Weijia Zhou (born in 1957) is currently a Professor at Shenyang Institute of Automation, Chinese Academy of Sciences, China. His research interests include robotics, mechachonics engineering and man-machine system. Weijia Zhou is the corresponding author and can be contacted at: zwjsia@sina.com

Huijie Zhang (born in 1985) is currently an Associate Professor at State Key Laboratory of Robotics, Shenyang Institute of Automation, Chinese Academy of Sciences, China.

Wei Zhang (born in 1979) is currently an Associate Professor at State Key Laboratory of Robotics, Shenyang Institute of Automation, Chinese Academy of Sciences, China.

Guangxin Yang (born in 1987) is currently an Assistant Professor at State Key Laboratory of Robotics, Shenyang Institute of Automation, Chinese Academy of Sciences, China.